Composites Part B 281 (2024) 111549

Contents lists available at ScienceDirect

Composites Part B

journal homepage: www.elsevier.com/locate/composites

Characterisation of process-induced variability in wrinkle defects during double diaphragm forming of non-crimp fabric

A. Codolini [a], S. Chen [b], G.D. Lawrence [b], L.T. Harper [b], M.P.F. Sutcliffe [a,*]

[a] Department of Engineering, University of Cambridge, Cambridge, CB2 1PZ, UK
[b] Composites Research Group, Faculty of Engineering, University of Nottingham, NG7 2RD, Nottingham, UK

ARTICLE INFO

Keywords:
Finite element analysis
Double diaphragm forming
Non-crimp fabrics
Wrinkling defects
Variability

ABSTRACT

Experiments and numerical simulations are employed to determine the critical process variables that affect the quality of a two-layer biaxial non-crimp fabric (NCF) preformed using the double diaphragm forming (DDF) process. To prevent wrinkling defects, the process variables must be controlled, including the vacuum pressure, diaphragm tension, and ply-tool alignment. Inter-ply friction plays a critical role in the deformation mechanism, while the frictional interaction between the diaphragm and tool has a limited impact. The study also reveals that geometrical features have an impact on the variability induced by the forming process. Preforms deformed to tools with geometrical features of higher asymmetry or Gaussian curvatures reduce the uncertainty of the forming process by maintaining the same preform quality despite changes in forming variables.

1. Introduction

The Double Diaphragm Forming (DDF) process has become an attractive out-of-autoclave manufacturing process for preforming dry fabrics because of its ability to reduce costs and waste compared to autoclave moulding of unidirectional pre-preg tape laminates [1]. The DDF process involves compacting a dry fabric blank between a bottom and top elastomeric diaphragm with vacuum pressure. The air is evacuated between the bottom diaphragm and the forming tool, causing air pressure to shape the fabric material onto the tool's geometry.

The implementation of the DDF process for high volume applications (>1000 parts per annum) in near-net-shape manufacturing is currently held back by a limited understanding of the preforming variables that cause manufacturing defects. Manufacturing defects such as out-of-plane wrinkling require expensive corrections in highly automated factories [2] and significantly degrade the mechanical performance of the final composite part, reducing the composite mechanical strength by up to 70% [3]. In addition, manufacturing imperfections in the meso-scale alignment of carbon fibre bundles can result in local bending stresses. These stresses can cause a degradation of stiffness and a decrease in resistance to delamination within multi-layer non-crimp fabric (NCF) composites [4]. Furthermore, when NCF composites exhibit tow waviness, it results in the formation of resin-rich areas, which can have a detrimental impact on the compressive strength of the composite material [5]. To mitigate the formation of defects and to minimise the variability of DDF preforms quality, the mechanisms and processing variables that control the formation of defects have to be sufficiently understood.

There has been significant research exploring the mechanisms of defect formation during forming of dry and pre-preg fabrics, using both experimental approaches and the increasingly sophisticated numerical models of fabric forming. Thompson et al. [6], in a DDF study forming dry woven fabric over a tetrahedron, showed how early undulations in fabric shape initiated by bending stresses evolved into wrinkles, facilitated by the applied vacuum pressure. An experimental study by Hallender at al [7] of hot drape forming of a multilayer UD pre-preg stack to a 3D beam geometry showed how wrinkling associated with compression can occur even in a recess which would tend to promote tension in the fabric. Shearing in the fabric allowed it to deform better without visible defects. This work is complemented by a numerical study of the experimental setup by Sjölander et al. [8], who identified two mechanisms of wrinkling: global buckling associated with excess material, for example when forming into convex shapes, and local compression of single layers associated with shearing during forming, leading to buckling. Farnand [9] showed how, at a micro-level, intra-ply separation of fibres or rolling of fibres can lead to waviness or wrinkling, in 0° and 90° plies, respectively.

The importance of the interface between plies in multilayer forming is emphasised in several studies. Guzman-Maldonato et al. [10], in an experimental and modelling study, showed how changes in inter-ply friction affected the formability and wrinkling of dry fabric ply

* Corresponding author.
E-mail address: mpfs@eng.cam.ac.uk (M.P.F. Sutcliffe).

https://doi.org/10.1016/j.compositesb.2024.111549
Received 26 July 2023; Received in revised form 5 May 2024; Accepted 9 May 2024
Available online 22 May 2024

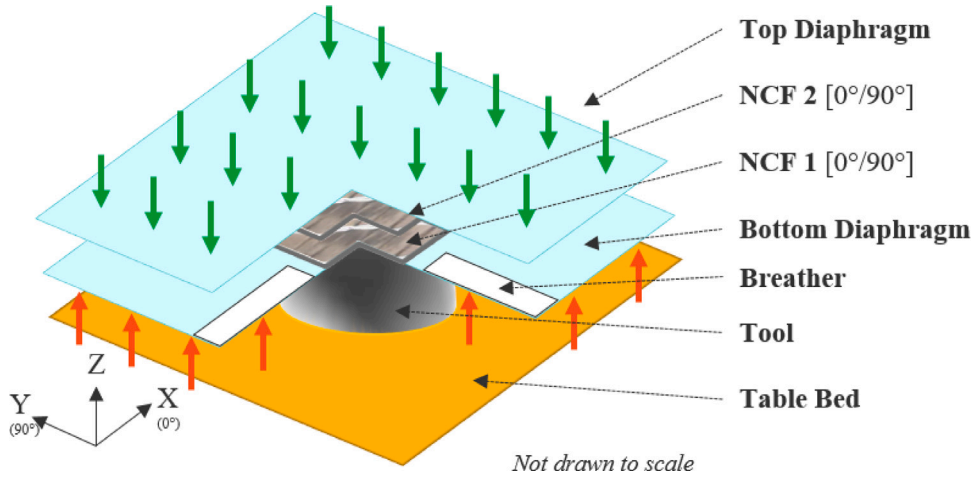

Fig. 1. The reference double diaphragm forming (DDF) setup, showing the NCF stack (NCF 1 and NCF 2) by removing a quadrant from the two diaphragms for clarity. Vertical arrows show the direction of the vacuum pressure used to form the NCF stack.

stacks. Locally reducing the frictional forces between the fabric stack and the diaphragm materials by means of liquid resin [11] was found to eliminate macroscopic defects such as wrinkles. The effect of interaction between plies affecting shear and wrinkling was characterised by Johnson et al. using a 'compatibility index' [12]. They showed that this index could explain changes in formability and wrinkling defects when using DDF to preform different pre-preg laminate layups into a spar geometry. These studies highlight the importance of inter-ply slip and fabric shear in affecting wrinkle formation, but show that wrinkling is also dependent on details of the materials, the part geometry and the forming process.

Since the mechanisms of defect formation depend on the details of the forming process, changes in these conditions can significantly change the likelihood of defects. In experimental studies of pre-preg preforming using a hot diaphragm forming rig, Bian et al. [13,14] showed how low temperature and high forming rate were responsible for increased wrinkling, which they associated with increased interply friction. Taking a more empirical approach, Yang and Colton [15] looked at the effect of lay-up on wrinkling in a dry fabric vacuum forming process, highlighting the effect of ply interfaces and part size on wrinkling. Their probabilistic approach to predicting wrinkling provides a rapid evaluation method which complements deterministic approaches.

Variations in process conditions can exacerbate the occurrence of defects by adding to the existing variability of tow orientation in dry fabrics [16]. In multi-ply forming, for example, the dry fabric layup can result in significant variations in wrinkling location and severity [17]. Only a small number of processing variables have been studied experimentally, due to the labour-demanding and time-consuming nature of experimental trials.

Numerical manufacturing tools, such as PAM-FORM, Aniform, and SIMUDRAPE, have been developed as stand-alone software or add-ons for commercial finite element method (FEM) codes. These simulation tools aim to accelerate the digitalisation of smart factories and to examine the impact of the manufacturing process on the structural behaviour of composite materials [18]. However, there has been a lack of research in utilising the precision of these FEM codes to explore the uncertainties associated with the manufacturing of dry fabrics. One example is given by Yu et al. [19], who showed how variations in fibre architecture can influence the forming behaviour of NCF preforms. By implementing a stochastic model of the fibre angle with a normal distribution with a mean angle of 90° and a standard deviation of 1° the number of wrinkles was reduced and the maximum shear angle dropped by 30%.

2. Scope of the paper

The above introduction details the importance of wrinkle prediction in preforming of dry fabrics but highlights the lack of research identifying the factors affecting process variability. Hence the present work aims to assess the variability in wrinkle formation due to process variability during preforming of NCFs using DDF. This is addressed using a mixture of finite element (FE) modelling and experimentation. Although other forms of defect including bridging and gapping are relevant, the focus of this paper is on wrinkling defects as this is a key form of defect which is likely to vary significantly and in less predictable ways with process variables. In addition, wrinkling defects cannot be eliminated by post-forming operations like trimming or local reinforcements as per bridging or gapping defects, respectively.

The base reference case ('REF') used in the work is illustrated in Fig. 1, showing DDF of a two-layer NCF preform over a hemispherical tool. Finite element modelling is used to explore the roles of the following process variables on the variability in wrinkle formation: vacuum pressure, diaphragm pre-tensioning, ply-tool misalignment and friction at the three interfaces (between the tool and diaphragm, between the plies and at the ply-diaphragm interface). Experiments are used to complement this numerical study. Fig. 2 illustrates the range of process variables considered in the study and Table 1 gives a summary of aspects used to examine the effect of process variables for the reference geometry. Although the FE model used has already been published and validated using a stepped-spar geometry [20], the overlap of conditions between the numerical and experimental strands of the study provides an opportunity to check on the level of accuracy of the predictions.

The effect of tool geometry on wrinkling variability is considered via numerical modelling, considering the effect of changes in ply-tool misalignment and vacuum pressure. Again this is complemented by the experimental study. Table 2 gives a summary of conditions considered in this part of the study.

The following section describes the methodologies for the numerical and experimental studies. Results for the effect of process conditions and the influence of geometry are presented in Sections 4.1 and 4.2 respectively. The discussion section further elaborates on these results and their implications for improving the repeatability of the DDF. Finally, the conclusion section outlines the main findings of the study.

3. Methodology

This section describes the materials, geometry, and forming details for both the numerical and experimental strands to the paper, along with the methods used to extract and characterise the wrinkle defects.

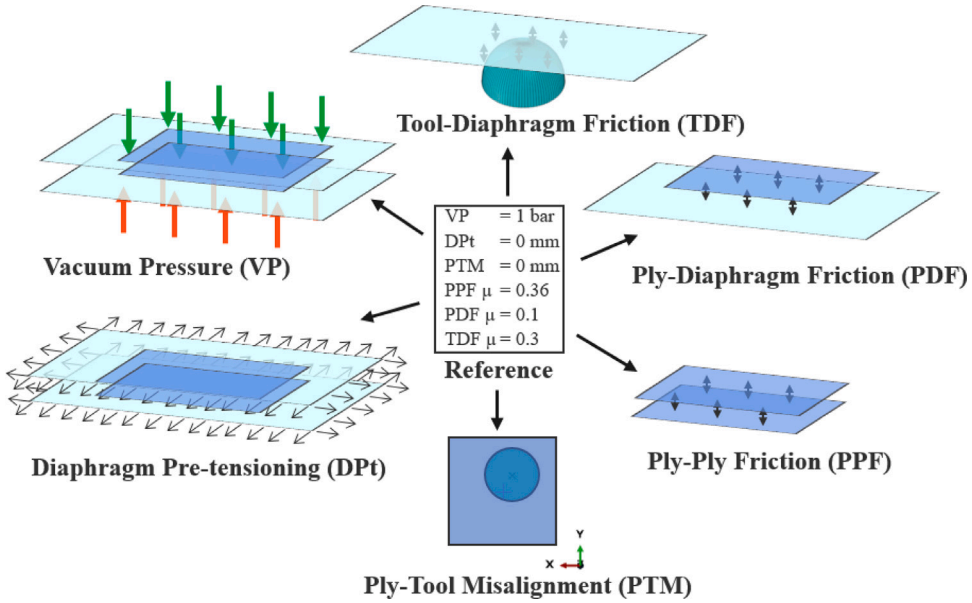

Fig. 2. Outline methodology of the numerical simulations conducted to investigate the impact of changing process parameters from a reference value on the variation in wrinkling defects during the DDF. Coulomb friction coefficients μ are quoted in the Reference box.

Table 1
Overview of the numerical and experimental cases considered to investigate the effect of process variables for the reference hemisphere geometry.

Variable	Reference value	Variation considered	Method used
Vacuum pressure	1 bar	±10%	Numerical
Diaphragm pre-tensioning	No pre-tension	Up to 50 mm stretch	Numerical
Tool-diaphragm friction coefficient	0.3	±10%	Numerical
Ply-diaphragm friction coefficient	0.1	±10%	Numerical
Ply-ply friction coefficient	0.36	±10%	Numerical
Ply-tool misalignment	No misalignment	Up to 20 mm	Numerical
Ply-tool misalignment	No misalignment	Up to 15 mm	Experimental

Table 2
Overview of the numerical and experimental cases considered to investigate the effect of tool geometry.

Variable	Process variation considered	Geometry	Method used
Vacuum pressure	1 bar ± 10%	Reference and 12 alternate geometries	Numerical
Ply-tool misalignment	Up to 15 mm	Reference and 12 alternate geometries	Numerical
Ply-tool misalignment	Up to 15 mm	Reference and high Gauss curvature	Experimental

3.1. Materials

The fabric material used in the experiments was a carbon fibre bi-axial ±45° NCF with texturised polyester pillar stitches, manufactured by Hexcel Ltd with material code FCIM359. Two plies in a [0°/90°, 0°/90°] layup were investigated to allow consideration of the effect of inter-ply friction on the preform quality. Each NCF ply was 0.4 mm thick and had a nominal areal weight of 441 gsm.

The top and bottom diaphragms, which apply the forming pressure to the fabric blank, were made from a high elongation thermoplastic vacuum bag film (StretchLon HT-350), supplied by Tygavac Ltd UK. Each layer of the thermoplastic material was 0.08 mm thick and the size of each diaphragm was 1.8 m × 1.5 m.

The same materials used in the experiments are modelled in the numerical simulations. Details of how these materials were modelled are described in Section 3.3.2.

3.2. Tool geometries

The tool geometry used as a reference for both the experimental and numerical studies was a 50 mm radius hemisphere. This was chosen as a geometry commonly found in the literature which can generate wrinkles during preforming, while being a symmetric geometry defined by a double curvature with no sharp corners. However it is clear that geometrical features of the tool considerably influence the formation of wrinkles during preforming. Hence the effect of a range of geometries on wrinkle variability was considered for both the experimental and numerical studies.

In the numerical study the investigation of the effect of vacuum pressure and ply-tool misalignment on wrinkle variability was conducted on twelve geometries in addition to the reference hemisphere. These geometries were chosen as a subset of the many considered in a preforming study by Viisainen et al. [21]. These geometries, which were generated by connecting a series of polygons, were all convex and had a constant height, but had shapes with extreme values for the following metrics:

- conicity: the mean overall draft angle between the top and the bottom polygons.
- asymmetry: measured by the offset distance from the centre of the tool.
- mean curvature: averaged over the geometry surface.
- angularity: calculated using the mean interior angle of the polygons.
- tortuosity: quantified by the largest relative twist within the geometry.

Table 3
Details of the linear regression models used to define the wrinkle amplitude difference for each forming variable. Regression coefficients are given for the predicted change in wrinkle amplitude, expressed as a percentage of the wrinkle amplitude for the reference case, with a change in the given process variable, again expressed as a percentage of the reference value. The diaphragm pre-tensioning stretch is expressed as a percentage of the diaphragm width (500 mm) and the ply-tool misalignment is expressed as a percentage of the ply width (200 mm).

Variable	Regression coefficient	Coefficient of determination (R^2)
Vacuum pressure	1.34	0.75
Diaphragm pre-tensioning	−3.10	0.91
Tool-diaphragm friction coefficient	0.94	0.61
Ply-diaphragm friction coefficient	0.022	0.60
Ply-ply friction coefficient	2.41	0.85
Ply-tool misalignment	0.94	0.68

- Gauss curvature: averaged over the geometry surface

These twelve geometries are illustrated in Fig. 3, showing how the changes in shape metrics translate into a broad range of geometries. Further details of the metrics and geometry generation methodology are given in [21].

For the experimental study, in addition to the hemisphere shape, the effect of geometry was considered by using the tool shape with the highest Gaussian curvature, as illustrated in Fig. 3. This had an asymmetric geometry and featured two ramps with distinct curvatures along its height. Both ramps measured 50 mm in height, defining the tool's overall height. Hence this shape is more representative of industrial applications than the hemisphere as it incorporates ramps and flat surfaces commonly found in components such as aerospace wing spars.

The tools were manufactured for the experimental study using epoxy tooling board material EB700 supplied by Easycomposites Ltd. To minimise damage to the bottom diaphragm during the forming trials, all tool edges were smoothed with 2 mm radius fillets. The hemispherical tool was machined from a 500 mm × 500 mm × 100 mm epoxy tooling board, causing its base to be elevated by 50 mm from the forming rig's bed. The double ramp tool was machined from a 50 mm × 60 mm × 50 mm epoxy tooling block.

3.3. Forming process details

This section describes details of the forming process for both the numerical simulations and the experiments. Details of the process variables considered in the study are given in the following section.

3.3.1. Experiments

The experiments used the laboratory-scale DDF rig designed by Chen et al. [22], as shown in Fig. 1. The two aligned fabric plies were enclosed between the two 1.8 m × 1.5 m diaphragms. The fabric blank had dimensions 200 mm × 200 mm to ensure that the deformed fabric covered the entire tool area, minimising the impact of edge effects. A breather cloth was placed between the two diaphragms to ensure that the air between the diaphragm materials was removed during the entire forming process, allowing for uniform pressure to be applied to the dry fabric and shape it onto the tool. For each forming experiment, three repetitions were conducted to provide statistical data for the results.

3.3.2. Numerical modelling

The FE software ABAQUS/Explicit was used to simulate the DDF process, following closely the approach detailed by Yu et al. [20].

The NCF fabrics were modelled using a shell-based approach, first introduced by Yu et al. [23] and experimentally validated for a wing spar geometry by [20]. This uses a non-orthogonal constitutive model [23] with each ply modelled by a laminated shell element comprising three layers, the central one controlling in-plane tensile and shear behaviour and the outer layers controlling the bending behaviour, assumed constant. The material model was implemented through a user defined fabric material subroutine. The material properties of the elements were defined based on a series of coupon tests which measured the in-plane and bending properties of the fabric. Further details are given in [20].

The diaphragm material was modelled using hyperelastic shell elements, with the specific material properties defined by in-plane tests as described by Yu et al. [20]. To reduce the computational cost a reduced size of 500 mm × 500 mm was used for the diaphragm and the breather material was not simulated. Vacuum pressure loading was simulated using normal pressure loads on the diaphragms.

The numerical model employed reduced quadrilateral shell elements (S4R) with a 3 mm edge size, which was found in the previous studies using this FE approach to give sufficient accuracy for wrinkle prediction with thin laminates while being computationally efficient. Again further details of the modelling approach are detailed in [20].

3.4. Process changes

The numerical modelling approach allows examination of the effect of a range of process variables on the variability in the induced wrinkle formation. Additionally a more limited set of experimental tests examined the effect of ply-tool misalignment.

For the numerical simulations of changes in process variable, scatter was observed in the way that wrinkle formation changed with changes in the process variable. This is associated with the somewhat random nature of the wrinkle formation. Hence a number of simulations were undertaken for each change of process variable, linearly spaced to span the range of the process variable considered. A linear regression fit to the data was made to quantify the effect of the given process variable. This fit was then used to find the change in wrinkle amplitude and position expected due to the maximum change in the given variable. Values for the R^2 regression coefficient across the range of process variables were in the range 0.60 to 0.91, as detailed in Table 3.

3.4.1. Vacuum pressure

Vacuum pressure plays a crucial role in the DDF process, as it helps to compact the dry fibres within the diaphragms and transmits hydrostatic pressure to deform the blank to the required tool shape. To study the impact of vacuum pressure on wrinkling defects in the numerical study, the magnitude of the vacuum pressure was altered by ±10% of its reference value of 1 bar. The effect of vacuum pressure was considered in this way for the reference hemisphere tool and the twelve alternate geometries. Although in practice a vacuum pressure greater than 1 bar is not realistic, this approach still captures the effect of a change in this variable effectively. Twenty simulations were used to span the ±10% range in the reference pressure.

3.4.2. Diaphragm pre-tensioning

The onset of wrinkling in dry fabrics during the DDF process is driven by material draw-in. When the material is subjected to global [24] or local [25] tension by stretching the diaphragms, it is possible to reduce the wrinkling severity. Hence, the effect of diaphragm pre-tensioning, induced by stretching the edges of the diaphragm prior to forming, on the forming quality of non-crimp fabrics was investigated in the numerical study. Before starting the forming process in the FE simulation, a displacement was applied to the edge nodes of both diaphragm to stretch them in the x–y plane. Ten simulations with stretches of up to 50 mm were applied, corresponding to a strain of the diaphragm of up to 10%.

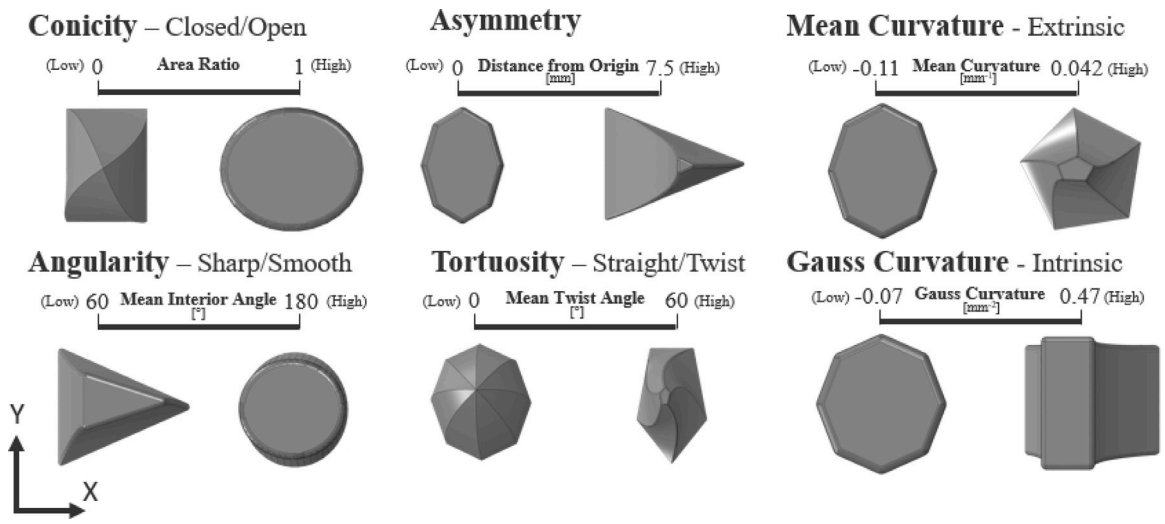

Fig. 3. Collection of tool shapes examined to analyse the change in process-variability due to the tool geometry in the DDF. The minimum (Low) and maximum (High) values of each geometrical feature were obtained from Viisainen et al. [21]'s numerical study.

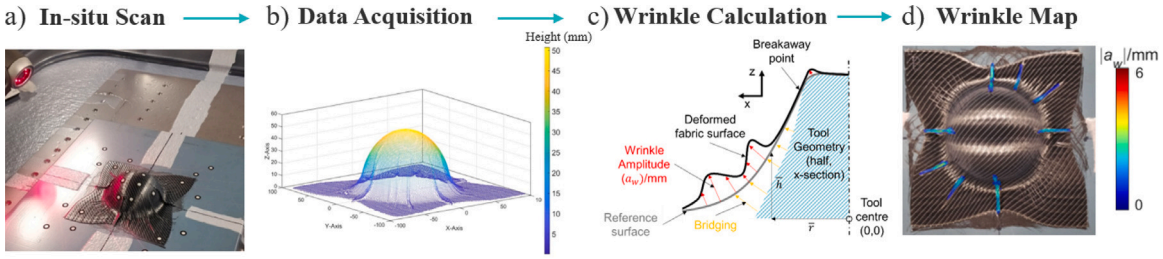

Fig. 4. An outline of the method used for calculating the wrinkle map from each DDF experimental trial. (a) The fabric preform was scanned in situ while the vacuum pressure was holding the deformed shape. (b) From the scanned data point cloud, a MATLAB code was developed to define the boundaries of the preform and align it to the machine bed (x–y plane). (c) The wrinkle amplitude at each point on the fabric surface was calculated using the methodology developed by Viisainen et al. [17] to filter out the bridging defects from the deformed fabric surface. (d) The wrinkle map was then projected onto DDF preform images.

3.4.3. Friction

As discussed in the introduction, friction plays a significant role in affecting slip between the various components in the process and hence changing the forming behaviour. In the numerical investigation, a penalty contact algorithm was used with a Coulomb friction model. The reference values of the friction coefficients used were $\mu_{tool-dia} = 0.3$, $\mu_{ply-dia} = 0.1$, $\mu_{ply-ply} = 0.36$ for tool-diaphragm friction, ply-diaphragm friction, and ply-ply friction, respectively. To investigate the impact of friction on wrinkling defects, the nominal values of these friction coefficients were changed with 20 simulations spanning ±10% of their reference values.

The friction coefficient for the critical ply-ply interface has been experimentally measured using a sled test (ASTM D1894, withdrawn in March 2023). Details of the measurements are given by Yu [11,26], who found that a Coulomb friction model fitted the data well, with a friction coefficient in the range 0.3 to 0.4 depending on the relative ply orientation and sliding direction. The value we use of $\mu_{ply-ply} = 0.36$ reflects this measured data. These references also included sled-test measurements for the ply-diaphragm and tool-diaphragm interfaces, deducing Coulomb friction coefficients of 0.4 and 0.25, respectively. The value we use for these interfaces of 0.1 and 0.3 differ from those measurements but, while the absolute accuracy of the wrinkle predictions will be affected by the choices of reference friction coefficients for the diaphragm interfaces, the aim of the paper, to explore the effect of changes in these variables, is not significantly affected.

3.4.4. Ply-tool misalignment

Changes in the alignment of the dry fabric blank relative to the tool may change the details of how the fabric drapes over the tool and hence the wrinkle formation and variability in wrinkling. This aspect of the process was considered both in the numerical and experimental parts of the work. The effect of a misalignment along one axis of the blank was considered. In practice the direction as well as magnitude of the misalignment will be important but considering this further complication was beyond the scope of this study.

The ply-tool misalignment was quantified by the distance Δ_{PTM} between the centre of the flat ply blank and the centroid of the tool area projected onto the ply blank. In the numerical study the misalignment was varied with ten simulations up to a maximum distance $\Delta_{PTM} = 20$ mm (equivalent to 10% of the ply width). This study was repeated for the reference hemisphere tool and the twelve alternate geometries.

The effect of ply-tool misalignment was similarly examined experimentally. For the hemisphere case, two different levels of ply-tool misalignment ($\Delta_{PTM} = 10$ mm, 15 mm) were compared to the reference case with no misalignment ($\Delta_{PTM} = 0$ mm). For the asymmetric double-ramp tool, both positive ($\Delta_{PTM} = 10$ mm, 15 mm) and negative ($\Delta_{PTM} = -10$ mm, -15 mm) levels of misalignment along the direction of the ramp were considered due to the asymmetric design of the tool.

3.5. Quantification of wrinkle variability

This section describes the method used to characterise the wrinkles and hence quantify the variability in wrinkle formation. A similar approach is adopted for both the numerical and experimental studies, once the geometry of the tool and deformed fabric has been identified.

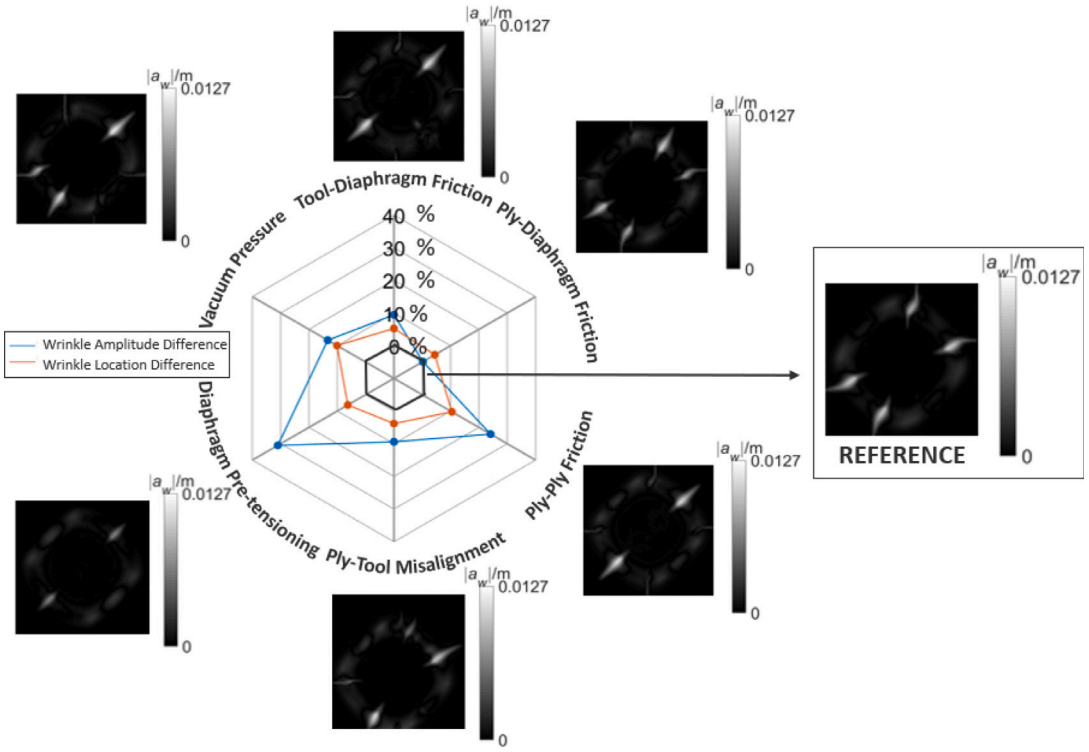

Fig. 5. A polar chart diagram of the percentage change in wrinkle amplitude (shown in blue) and wrinkle location (shown in orange) difference compared to the references conditions for the following forming variables: tool-diaphragm friction, ply-diaphragm friction, ply-ply friction, ply-tool misalignment, diaphragm pre-tensioning, and vacuum pressure. The wrinkle amplitude is expressed as a percentage of the wrinkle amplitude for the reference case, and the plot gives the expected change for a 10% change in the given process variable. The wrinkle location change is expressed as a percentage of the hemisphere radius, and is given as the mean location change with a ±10% change in the given process variable. The most extreme case in wrinkle amplitude difference of each forming variable is displayed outside each segment of the diagram via 2D grayscale representations of the projected wrinkle map. The brightest shade in the image represents the highest level of wrinkle severity. (For interpretation of the references to colour in this figure legend, the reader is referred to the web version of this article.)

3.5.1. Measurement of wrinkles

To measure wrinkles in the experimental set-up, first a 3D in-situ laser scanner (Creaform HandySCAN 700 Elite) was used to obtain 3D point cloud data of the preform's deformed shape whilst still maintaining the vacuum. The tool was also scanned. A MATLAB code was developed to reconstruct the preform's coordinates and align them parallel to the tool base as shown in Fig. 4b.

For the numerical modelling, the geometry of the tool and deformed fabric could be extracted directly from the simulations.

3.5.2. Characterisation of wrinkles

The process for characterising wrinkles was common to the numerical and experimental strands, once the tool and deformed shape had been extracted. The first step in the wrinkle characterisation was to extract the wrinkle amplitude from the deformed fabric shape. This used the methodology described by Viisainen et al. [17]. A wrinkle-free reference surface was calculated by combining a bi-directionally smoothed geometry of the preform with the geometry of the tool. The deviation of the deformed fabric from this wrinkle-free reference surface (Fig. 4c) was found and used to calculate the wrinkling and bridging defect components of the difference in the surfaces. The wrinkle component of the difference gives the variation of local wrinkle amplitude $a_W(i)$ over the surface. This wrinkle amplitude variation was then mapped back onto the undeformed fabric, to generate a 2D wrinkle map which could be represented in the form of a grayscale image. In addition these wrinkle amplitudes could be projected onto the deformed fabric geometry, as illustrated in Fig. 4d. To ensure that only visible and significant wrinkles were included in the average wrinkling and wrinkle area calculations, a 1 mm threshold in the wrinkle amplitude a_W was introduced.

Three wrinkle amplitude parameters were defined to characterise wrinkling:

- maximum wrinkling amplitude $a_{MAX} = max(a_W(i))$,
- average wrinkling amplitude $\bar{a}_W$: the arithmetic mean of the wrinkle amplitudes a_W within the parts of the surface containing wrinkles,
- wrinkle area A_W: the total area of wrinkles, as mapped back to the undeformed fabric, divided by the total area of the undeformed fabric and expressed as a percentage.

Finally, to quantify the variability in wrinkling, we need a procedure to compare different wrinkle patterns. Here we adopted the process introduced by Viisainen et al. [17], who used an image analysis methodology to compare wrinkle patterns. By mapping all the wrinkle patterns back onto the undeformed blank, the results for a given forming test can be captured by a grayscale map of the amplitude of the wrinkle as a function of the location on the blank (as shown for example in the grayscale images of Fig. 5). Then the difference between any two images, corresponding to two wrinkling patterns, can be represented by a non-rigid registration of one image to the other. In this procedure all the pixels in the 'moving image' were adjusted systematically in terms of intensity and position so as to map onto the 'fixed image'. The wrinkle amplitude difference Δa_W was found from the absolute difference between the average wrinkle amplitude $\bar{a}_W$ of each grayscale image. The wrinkle location difference Δl_W was found by taking the maximum required pixel movement in mapping one wrinkle image to the other.

4. Results

This section details the effects of process changes and tool geometry on the variability in wrinkle formation during the DDF pre-forming, combining results from the numerical and experimental studies.

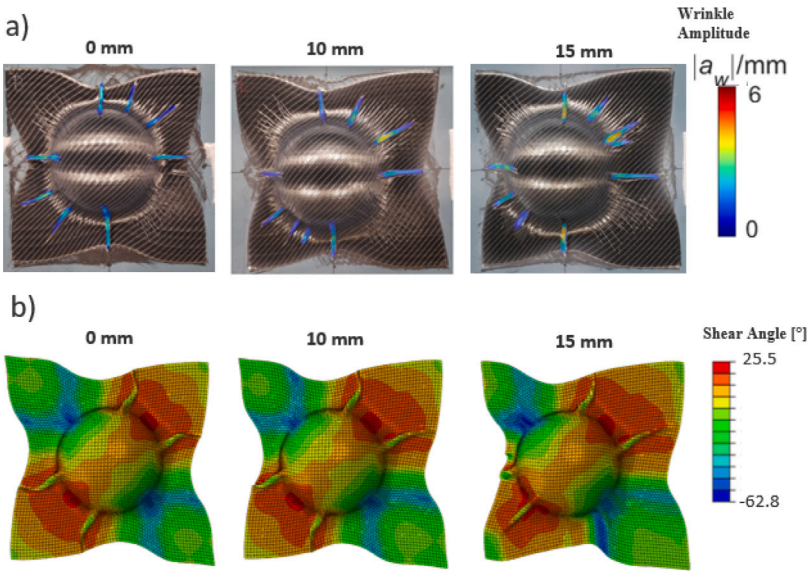

Fig. 6. The results of the ply-tool misalignment test are shown for the DDF of a 50 mm radius hemispherical tool geometry. For each misalignment level, (a) the experimental deformed shape is displayed along with the wrinkling amplitude severity and (b) the numerical deformed shape is plotted with the shear angle contour plot.

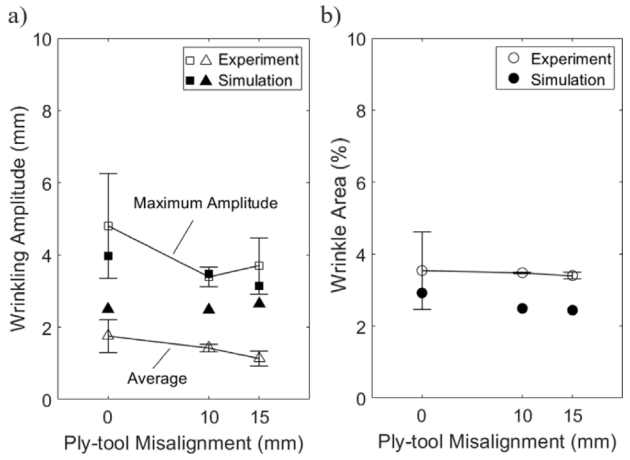

Fig. 7. Influence of the ply-tool misalignment on the wrinkling defect for the DDF of a 50 mm radius hemispherical geometry. (a) The maximum and average wrinkling amplitude and (b) the wrinkle area are displayed. For each ply-tool misalignment level, the mean value (empty marker) and standard deviation bar of three experimental repetitions are compared to the simulation result (solid marker).

4.1. Effect of process changes

The numerical modelling approach was used to explore the role of the following process variables on the variability in wrinkle formation: vacuum pressure, diaphragm pre-tensioning, ply-tool misalignment and friction at the three interfaces (between the tool and diaphragm, between the plies and between the plies and diaphragm). For each forming variable change, the mean wrinkle amplitude difference Δa_W and mean wrinkle location difference Δl_W were calculated when compared with the reference forming conditions. A regression fit to the simulations gives the expected change in the wrinkle amplitude or location due to a change in the given process variable, as defined by Table 1. The regression coefficient is given as the rate of change in the wrinkle amplitude, expressed as a percentage of the wrinkle amplitude with reference conditions, with the change in the given process variable, again expressed as a percentage of the original value. The pre-tensioning stretch is expressed as a percentage of the diaphragm width, i.e. to give a nominal strain. The ply-tool misalignment is expressed as a percentage of the ply width (equal to 200 mm). A positive value for the regression coefficient corresponds to an increase in the wrinkle amplitude for an increase in the corresponding variable. Only diaphragm pre-tension has a negative coefficient, with wrinkle amplitude decreasing with an increase in pre-tensioning stretch. These results are summarised in the polar chart in Fig. 5, with the two lines plotting the amplitude and location differences for the different process changes. The amplitude differences are plotted as the expected change in the wrinkle amplitude, as a percentage of the wrinkle amplitude for the reference conditions, with a maximum (i.e. 10%) difference in the given process variable. The location difference is plotted as the average wrinkle location difference for a given change in process variable (i.e. averaging results for the ±10% change in process conditions), expressed as a percentage by dividing by the hemisphere tool radius (50 mm).

Fig. 5 shows that the most influential process variable from the numerical study affecting the wrinkle amplitude was pre-tensioning of the diaphragm material prior to forming (Δa_W = 31%). This was followed in importance by inter-ply friction (Δa_W =24%). The remaining factors (ply-tool misalignment, vacuum pressure, diaphragm-tool friction and diaphragm-ply friction) had a smaller effect on variability in the wrinkle amplitude.

The results from the numerical study for the variability in wrinkle location are also included on Fig. 5. Here the most influential process variables were seen to be inter-ply friction and vacuum pressure. The other process parameters had a smaller but not insignificant effect on wrinkle location. In this study the two plies were aligned with each other, resulting in similar deformation patterns in the plies. Use of differing ply orientations would increase slip between plies and likely further increase the effect of friction between plies on wrinkle variability.

The numerical results for the effect of ply-tool misalignment on wrinkling were supported by the experimental study of this process variable for the reference hemisphere geometry. Fig. 6a, which projects the wrinkle amplitude onto an image of the deformed preform, showed that there was a consistent wrinkle pattern regardless of the degree of misalignment. The cross-like wrinkles appeared consistently across the equator, and shear-induced wrinkles formed in the first and third quadrants where positive shear angles were observed. The experimentally observed changes in wrinkle amplitude and area are plotted in Fig. 7, showing how the amplitude tended to decrease with increasing misalignment while the area remained relatively fixed.

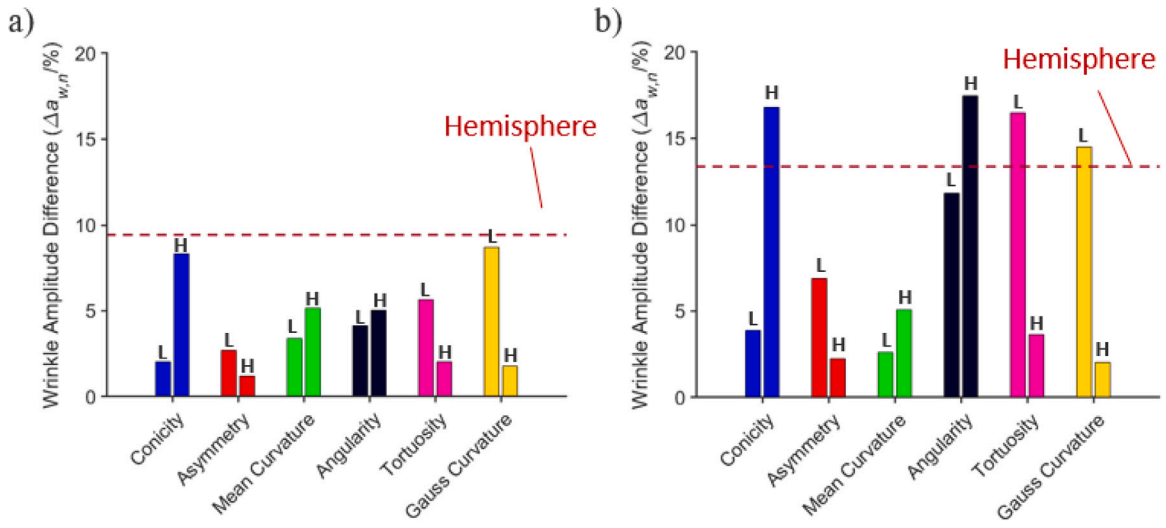

Fig. 8. Bar chart plots showing the impact of the six geometrical characteristics (Low and High), introduced in Fig. 3, on the wrinkle amplitude difference for (a) the ply-tool misalignment and (b) forming vacuum pressure. For each tool geometrical characteristic, the wrinkle amplitude difference is calculated as the mean difference for small changes (from 1% to 10%) in forming variables compared to the reference case. The forming variables in the reference configuration are presented in Fig. 2. The wrinkle amplitude difference for the hemisphere case is highlighted by a dashed red line in each graph.

Corresponding numerical predictions of the wrinkle pattern and change in wrinkle metrics are given in Figs. 6b and 7, respectively. The numerical model accurately predicted the maximum wrinkling amplitudes caused by shear locking (Fig. 7a), as they developed in the area of positive shear angle. However, it failed to capture the cross-like wrinkles, resulting in an underestimation of the wrinkle area by 18% for all ply-tool misalignment levels, as shown in Fig. 7b. Although the origin of these cross-wrinkles in the experiments is not clear, additional experiments with different breather configurations showed a change in the amplitude of these wrinkles, indicating that the interaction between the breather and diaphragm deformations at these locations may be influencing this wrinkle behaviour.

4.2. Effect of tool geometry

Fig. 8a presents numerical results for the impact of the tool geometrical features on the wrinkle variability induced by ply-tool misalignment. Results are presented for geometries with low (L) or high (H) values of the metrics used to characterise the geometry. Fig. 8a shows that the variability in wrinkle amplitude induced by a ±10 mm ply-tool misalignment was smaller for all the alternate geometries as compared with the reference hemisphere. Geometries with high conicity and low Gaussian curvature exhibited behaviour more similar to the hemisphere due to the circular features of these tools. The induced changes in wrinkle amplitude were least for the high asymmetry and high Gauss curvature tools.

Turning to the predicted variability due to changes in vacuum pressure, Fig. 8b shows that some geometries now had more variable wrinkling than the reference hemisphere, including geometries with high conicity or angularity. Again the high asymmetry and high Gaussian curvature geometries showed the least change in wrinkle amplitude associated with this process change.

Experiments measured the effect of ply-tool misalignment for the high Gaussian curvature double-ramp geometry. As with the reference hemisphere, the observed location of wrinkles was consistent across all levels of misalignment, see Fig. 9a. The presence of the observed out-of-plane wrinkles in positive shear angles regions was accurately predicted by the numerical model. Furthermore the numerical model successfully captured the maximum wrinkle amplitude for each ply-tool misalignment level, although the area of wrinkles was somewhat underpredicted compared with experiments (Fig. 9). These experimental results confirmed the insensitivity of the maximum wrinkle amplitude to ply-tool misalignment seen in the numerical modelling for this tool geometry, see Fig. 10a. This insensitivity to ply-tool misalignment for the high Gaussian curvature geometry differs from the results for the hemisphere reference tool, Fig. 7a, where both experiments and predictions showed a tendency for the wrinkle amplitude to fall with increasing misalignment. Note that the latter effect of reduced wrinkling with increased misalignment is to some extent a function of the limited size of the blank, and may not be typical of preforming with larger blanks. Similarly it is expected that the change in wrinkle variability could change significantly with the direction of the ply-tool misalignment.

The predicted difference of the effect of geometry on variability for ply misalignment compared with vacuum pressure was unexpected, as was the finding that the reference geometry was most sensitive to tool misalignment. In retrospect it may have been useful to use another geometry as a reference, but in any case the comparison of the different geometries, particularly for the numerical results, highlights the importance of the interplay of geometry and process parameters on variability.

5. Discussion

5.1. Assessing forming variability

In the DDF process, there are many process variables that affect the quality of pre-formed fabrics and the variability in wrinkling. This study has shown that a combination of experiments and numerical simulations can effectively explore the effect of forming variables on the variability in wrinkle formation.

Based on the numerical analysis (Fig. 5), operating guidelines for improving the repeatability in forming dry fabric materials can be established. Firstly, inter-ply friction significantly affects the variability in wrinkle formation in forming a multi-ply stack. Thus it will be important to control fabric surface quality and other factors such as temperature or binder quantity which could affect this friction component. On the other hand, the friction between the tool and the bottom diaphragm has a lesser impact on product quality.

Results show that tensioning of the diaphragm material strongly influences the formation of wrinkling in dry fabric forming, with changes in tension significantly influencing variability. Introducing risers in the machine setup, as suggested by Chen et al. [27], can help control local tensioning of the diaphragm.

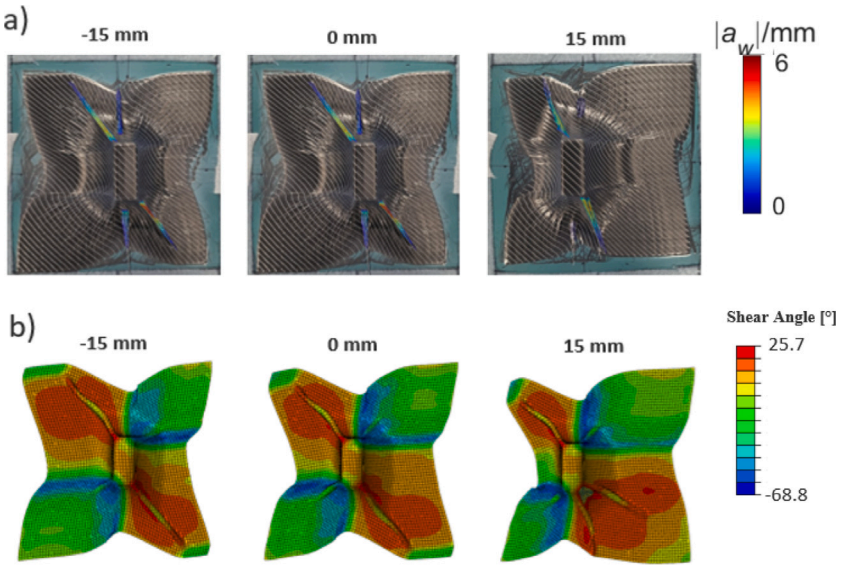

Fig. 9. The results of the ply-tool misalignment test are shown for forming of the tool geometry with the highest Gaussian curvature in Fig. 3. For each misalignment level, (a) the experimental deformed shape is displayed along with the wrinkling amplitude severity and (b) the numerical deformed shape is plotted with the shear angle contour plot.

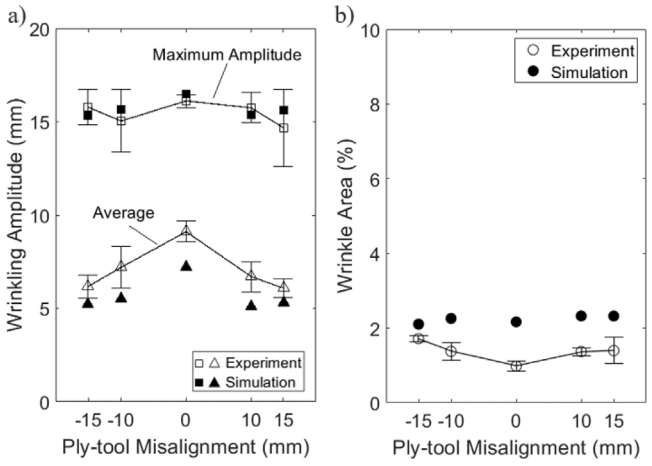

Fig. 10. Influence of the ply-tool misalignment on the wrinkling defect formation for forming of the tool geometry with the highest Gauss curvature in Fig. 3. (a) The maximum and average wrinkling amplitude and (b) the wrinkle area are displayed. For each ply-tool misalignment level, the mean value (empty marker) and standard deviation bar of three experimental repetitions are compared to the simulation result (solid marker).

Finally the study indicates that vacuum pressure and ply-tool misalignment affect wrinkle amplitude differences in hemisphere forming to a lesser extent than the other process variables.

Fig. 5 provides a quantitative measure of the influence of different forming variables on the variability in wrinkling in DDF preforms, representing the change in wrinkling associated with the maximum change in the process variables as defined by Table 1. By setting an acceptable variability in wrinkling location and amplitude, this could be used to set acceptable variabilities in the different process variables. For example setting a threshold of 10% in wrinkle amplitude variability would correspond to an acceptable change in the vacuum pressure of 7.5%, slightly less than the maximum applied in the study. However ply-ply friction needs to be restricted to vary by less than about 4% to keep the variability of the amplitude of wrinkles below 10%.

We note that the friction approach used simplifies the friction modelling. The nominal friction coefficient is expected to depend on the slip distance and direction, pressure and fabric orientation. Recent work using a vacuum bag arrangement has generated improved estimates of friction [28], by measuring the sliding resistance when the fabric layers are pressed together using a vacuum bag arrangement rather than at lower pressures in the sled test. Nevertheless, while the details of the friction modelling are rather approximate, the conclusions relating to the importance of friction on wrinkle variability should still be valid.

Although the above observations are based on results for the studied biaxial NCF material, the numerical method can be applied to other dry fabrics by incorporating an experimentally-validated constitutive model into the finite element simulation.

5.2. Improving manufacturing repeatability through component design

The repeatability in forming dry fabrics is significantly influenced by the shape of the tool geometry (Fig. 8), as certain geometric characteristics have a greater impact on the repeatability of the DDF process compared to others. When the tool geometry is highly asymmetrical, the forming quality of dry fabric preforms becomes more consistent. This is because the geometric features provide a specific direction for the development of wrinkling defects. On the other hand, when a very symmetrical shape is used, as with the hemisphere, no preferential directions are provided for the wrinkle to propagate, resulting in randomly occurring wrinkling defects in the region of positive shear deformations. Geometries with high Gaussian curvature, such as the double-ramp geometries studied in Section 4.1, exhibit lower sensitivity to changes in forming variables. These observations can guide the design of composite components, ensuring that the geometrical features are sufficiently separated from each other to prevent mutual influence.

6. Conclusions

This paper aims to assess the variability in wrinkle formation due to process variability during preforming of NCFs using DDF. This is addressed using a mixture of numerical modelling and experiments, considering a range of process variables and tool geometries.

Finite element simulations with the reference hemisphere geometry show that variability in pre-tensioning the diaphragm material prior to forming has the most effect on variability in the wrinkle amplitude. Variability in the friction coefficient between the fabric plies also contributes significantly to wrinkle amplitude variability.

The effect of variability of the process conditions on forming variability is influenced by the geometric characteristics of the tool. Tool

geometries with higher asymmetry or higher Gaussian curvatures are less susceptible to changes in the process variables considered (ply-tool misalignment and vacuum pressure) compared to geometries with larger angularity or conicity.

CRediT authorship contribution statement

A. Codolini: Writing – original draft, Methodology, Conceptualization. **S. Chen:** Writing – review & editing, Software, Investigation. **G.D. Lawrence:** Writing – review & editing, Investigation. **L.T. Harper:** Writing – review & editing, Supervision, Funding acquisition. **M.P.F. Sutcliffe:** Writing – review & editing, Supervision, Funding acquisition.

Declaration of competing interest

The authors declare that they have no known competing financial interests or personal relationships that could have appeared to influence the work reported in this paper.

Data availability

Data will be made available on request.

Acknowledgements

This work was funded by the Engineering and Physical Sciences Research Council (EPSRC), United Kingdom, as part of the EPSRC Future Composites Manufacturing Research Hub, via the grant number EP/P006701/1. The work conducted at the University of Nottingham was supported by the Made Smarter Innovation - Materials Made Smarter Research Centre [EP/V061798/1]. Yilong Li is acknowledged for helping operate the DDF machine at the University of Nottingham. The authors are also grateful for anonymous reviewers' comments. For the purpose of open access, the authors have applied a Creative Commons Attribution (CC BY) licence to any Author Accepted Manuscript version arising from this submission.

References

[1] Bibo GA, Hogg PJ, Kemp M. Mechanical characterisation of glass- and carbon-fibre-reinforced composite made with non-crimp fabrics. Compos Sci Technol 1997;57.
[2] Psarommatis F, May G, Dreyfus P, Kiritsis D. Zero defect manufacturing: state-of-the-art review, shortcomings and future directions in research. Int J Prod Res 2020;58:1–17.
[3] Potter K, Khan B, Wisnom M, Bell T, Stevens J. Variability, fibre waviness and misalignment in the determination of the properties of composite materials and structures. Composites A 2008;39:1343–54.
[4] Mattsson D, Joffe R, Varna J. Damage in NCF composites under tension: Effect of layer stacking sequence. Eng Fract Mech 2008;75.
[5] Drapier S, Wisnom M. Finite-element investigation of the compressive strength of non-crimp-fabric-based composites. Compos Sci Technol 1999;59.
[6] Thompson AJ, Belnoue JP-H, Hallett SR. Modelling defect formation in textiles during the double diaphragm forming process. Composites B 2020;202:108357.
[7] Hallander P, Akermo M, Mattei C, Petersson M, Nyman T. An experimental study of mechanisms behind wrinkle development during forming of composite laminates. Composites A 2013;50:54–64.
[8] Sjölander J, Hallander P, Åkermo M. Forming induced wrinkling of composite laminates: A numerical study on wrinkling mechanisms. Composites A 2016;81:41–51.
[9] Farnand K, Zobeiry N, Poursartip A, Fernlund G. Micro-level mechanisms of fiber waviness and wrinkling during hot drape forming of unidirectional prepreg composites. Composites A 2017;103:168–77.
[10] Guzman-Maldonado E, Wang P, Hamila N, Boisse P. Experimental and numerical analysis of wrinkling during forming of multi-layered textile composites. Compos Struct 2019;208:213–23.
[11] Yu F, Chen S, Harper L, Warrior N. Investigation into the effects of inter-ply sliding during double diaphragm forming for multi-layered biaxial non-crimp fabrics. Composites A 2021;150:106611.
[12] Johnson K, Butler R, Loukaides E, Scarth C, Rhead A. Stacking sequence selection for defect-free forming of uni-directional ply laminates. Compos Sci Technol 2019;171:34–43.
[13] Bian XX, Gu YZ, Sun J, Li M, Liu WP, Zhang ZG. Effects of processing parameters on the forming quality of C-shaped thermosetting composite laminates in hot diaphragm forming process. Appl Compos Mater 2013;20:927–45.
[14] Sun J, Gu Y, Li M, Ma X, Zhang Z. Effect of forming temperature on the quality of hot diaphragm formed C-shaped thermosetting composite laminates. J Reinf Plast Compos 2012;31(16):1074–87.
[15] Yang Y, Colton J. Statistical analysis and modeling of wrinkle defects in continuous-fiber composite forming processes. J Reinf Plast Compos 2023. 07316844231197251.
[16] Abdiwi F, Harrison P, Koyama I, Yu W, Long A, Corriea N, Guo Z. Characterising and modelling variability of tow orientation in engineering fabrics and textile composites. Compos Sci Technol 2012;72:1034–41.
[17] Viisainen J, Sutcliffe M. Characterising the variability in wrinkling during the preforming of non-crimp fabrics. Composites A 2021;149:106536.
[18] Frommel C, Haase T, Larse L, Vistein M, Willmeroth M. Digital factory. In: Design and manufacture of structural components. Woodhead Publishing; 2022.
[19] Yu W, Harrison P, Long A. Finite element forming simulation of NCF considering natural variability of fiber direction. In: Proceedings of the 8th international ESAFORM conference on materials forming, Cluj-Napoca, Romania. 2005.
[20] Yu F, Chen S, Harper L, Warrior N. Double diaphragm forming simulation using a global-to-local modelling strategy for detailed defect detection in large structures. Composites A 2021;147:106457.
[21] Viisainen J, Yu F, Codolini A, Chen S, Harper L, Sutcliffe M. Rapidly predicting the effect of tool geometry on the wrinkling of biaxial NCFs during composites manufacturing using a deep learning surrogate model. Composites B 2023;253:110536.
[22] Chen S, McGregor O, Endruewit A, Elsmore M, De Focatiis D, Harper L, et al. Double diaphragm forming simulation for complex composite structures. Composites A 2017;95:346–58.
[23] Yu F, Chen S, Viisainen J, Sutcliffe M, Harper L, Warrior N. A macroscale finite element approach for simulating the bending behaviour of biaxial fabrics. Compos Sci Technol 2020;191:108078.
[24] Krebs J, Friedrich K, Bhattacharyya D. A direct comparison of matched-die versus diaphragm forming. Composites A 1998;29:183–8.
[25] Chen S, McGregor O, Harper L, Endruewit A, Warrior N. Optimisation of local in-plane constraining forces in double diaphragm forming. Compos Struct 2018;201:570–81.
[26] Yu F. The prediction of wrinkle formation in non-crimp fabrics during double diaphragm forming (Ph.D. thesis), University of Nottingham, UK; 2022.
[27] Chen S, McGregor O, Harper L, Endruweit A, Warrior N. Optimisation of double diaphragm forming process through local adjustment of in-plane constraint. In: 21st international conference on composite materials. 2017.
[28] Lawrence G, Chen S, Warrior N, Harper L. The influence of inter-ply friction during double-diaphragm forming of biaxial NCFs. Composites A 2023;167:107426.